

DOI:10.1515/adms-2016-0016

**A. K. Krella, A. Krupa, A.T. Sobczyk, A. Jaworek**

*Institute of Fluid Flow Machinery, Polish Academy of Sciences, Fiszera 14,  
80-231 Gdansk, Poland  
akr@imp.gda.pl*

## **Al<sub>2</sub>O<sub>3</sub> + TiO<sub>2</sub> THIN FILM MADE BY ELECTROSTATIC SPRAY DEPOSITION**

### **ABSTRACT**

In this work electrostatic spray deposition process was used to deposit thin Al<sub>2</sub>O<sub>3</sub> + TiO<sub>2</sub> ceramic thin film on X10CrAlSi18 steel from colloidal suspension of TiO<sub>2</sub> powder in Al<sub>2</sub>O<sub>3</sub> precursor solution. The precursor was 3% solution of Al<sub>2</sub>(NO<sub>3</sub>)<sub>3</sub> in ethanol. An influence of the thermal treatment after film deposition on protective properties against high temperatures and film endurance were investigated. The resistance against thermal cycles and dynamic impacts were tested. Performed investigations showed that the best protective properties had the Al<sub>2</sub>O<sub>3</sub> + TiO<sub>2</sub> film sintered at 1000°C.

**Key words:** *ceramic coatings, thin film, fracture, electrostatic spray deposition*

### **INTRODUCTION**

Electrostatic spray deposition (electrospray, electrohydrodynamic atomization EHDA) is a method of thin film deposition at low cost. In this method thin film is made from liquid that is either colloidal suspension or is precursor solution. This deposition process is a physical process of aerosol generation by electrical forces that act on the surface of liquid at a capillary nozzle outlet. In case of using colloidal suspension, a size of particle powder has an influence on sedimentation process and thin film morphology. In case of using precursor solution, it undergoes decomposition during deposition or during thin film drying. Decomposition of precursor is often temperature dependent, so the substrate temperature plays an important role. As the substrates are heated, the formation of oxide thin films from precursor solution occurs directly on the substrate surface. Investigations of morphology of zirconia coatings [1] and La<sub>0.7</sub>Sr<sub>0.3</sub>MnO<sub>3</sub> coating [2] from precursor solution showed that thin film deposited at low temperature was cracked, while at high temperature very porous.

Aluminium oxide (Al<sub>2</sub>O<sub>3</sub>) is a hard ceramic compound, which has been investigated for high temperature applications because of its good thermal properties and good strength. Nevertheless, Al<sub>2</sub>O<sub>3</sub> has limited applications due to low ductility and low fracture toughness. Moreover, Al<sub>2</sub>O<sub>3</sub> coating, due to high melting point, is porous even after sintering. Therefore, to improve its properties and lessen coating porosity others compounds are added, e.g. addition of TiO<sub>2</sub> to alumina favours sintering Al<sub>2</sub>O<sub>3</sub> particles, and the rate of initial sintering increases approximately exponentially with titania concentration up to some limit beyond which sintering rate remains constant [3]. Moreover, during sintering a reaction between

titania and alumina occurs and aluminum-titanate structure having the composition of  $\text{Al}_2\text{O}_3$ - $\text{TiO}_2$  is formed. This compound has thermal properties useful for high temperature applications such as furnace linings. However, during its lifetime,  $\text{Al}_2\text{O}_3$  coating may undergo dynamic deformation; therefore it is important to investigate the resistance of a thin film against dynamic loading.

Slurry test is a simple and short-lasting method used to investigate the coating adhesion and resistance to dynamic load. Slurry tests belong to aggressive tests and cause severe erosion damage due to repetitive impacts of solid particles that flow with liquid. Resistance of materials against slurry erosion depends on material properties (hardness, stiffness, toughness), flow rate, kinetic energy of impacting solid particles, angle of impacts, property of solid particles, e.g. shape and hardness, and in case of coated materials, erosion rate depends on coating stiffness, hardness, thickness and adhesion to a substrate, and also on the mismatch between substrate and coating properties [4-9]. Depending on material stiffness the maximum erosion rate of material is reached at different impingement angle. In case of ductile material, the maximum erosion rate is reached at an angle of  $30^\circ$ , while in case of brittle materials at an angle of  $90^\circ$  [9,10]. The principal mechanism for material removal depends on material stiffness and also on the impact rate. In case of ceramic materials, to which  $\text{Al}_2\text{O}_3$  thin film belongs, they fractured in a brittle mode in the form of radial cracking.

The aim of this paper is to investigate the protective properties against oxidation in high temperature of  $\text{Al}_2\text{O}_3 + \text{TiO}_2$  thin film made from colloidal suspension of  $\text{TiO}_2$  powder particles in precursor solution by means electrostatic spray deposition method. For this purpose, resistance against cyclic annealing at  $1000^\circ\text{C}$  and resistance against dynamic loading of the  $\text{Al}_2\text{O}_3 + \text{TiO}_2$  thin film were investigated.

## EXPERIMENTAL

$\text{Al}_2\text{O}_3 + \text{TiO}_2$  thin films were deposited by EHDA process on ferritic X10CrAlSi18 steel. Substrate samples (40 x 10 x 4 mm) had rounded corners, with a radius of 5 mm, in order to avoid electrical discharges from sharp edges. Before coating, the substrates were thermally treated at  $800^\circ\text{C}$  for 1 h using Nabertherm L3/11 furnace in order to obtain their optimal thermal and mechanical properties. After thermal treatment substrates were sanded (sandpaper 220, 400 600 and 1000 SiC) and were washed using ultrasound. Then the roughness of substrates was measured using SJ-301 Mitutoyo Surface Roughness Tester. Mean Ra roughness parameter was  $R_a = 0.09 \mu\text{m}$  with a standard deviation of  $0.03 \mu\text{m}$ ,  $R_z = 0.70 \pm 0.28 \mu\text{m}$ .

$\text{Al}_2\text{O}_3 + \text{TiO}_2$  film was deposited from colloidal suspension that was made from  $\text{TiO}_2$  nanoparticles of mean size of 15 nm and precursor of  $\text{Al}_2\text{O}_3$ . As precursor was used a 3% solution of  $\text{Al}(\text{NO}_3)_3 \cdot 9\text{H}_2\text{O}$  in ethanol ( $\text{C}_2\text{H}_5\text{OH}$ , 99.9%). To 20 ml of precursor solution were added 31.5 mg of  $\text{TiO}_2$  nanoparticles (Alfa Aesar). The mixture of  $\text{TiO}_2$  particles and precursor solution was stirred for 24 hours and obtained colloidal suspension was electrostatically sprayed for a time of 90 min.

A schematic illustrating principle of electrostatic spraying used for coating deposition is shown in Fig. 1a. The ESD system consisted of stainless-steel capillary nozzle connected to high voltage supply SPELMANN SL600W/30kV/PN switched to positive polarity, and grounded metal collector on which a substrate was placed. Positive high voltage was 9.6 kV. The deposition mode was multi-jet (Fig. 1b). The diameter of capillary nozzle was 0.8 mm, and the distance between the nozzle tip and substrate was 16 mm. The flow rate of suspension

was 0.6 ml/h. The collector was designed as a turn-table to obtain more uniform deposition of the droplets onto the substrate. The collector was heated during the process of electrostatic spraying in order to obtain the substrate temperature of about 120°C to facilitate decomposition of aluminium nitrate nonahydrate (melting point is 74°C).

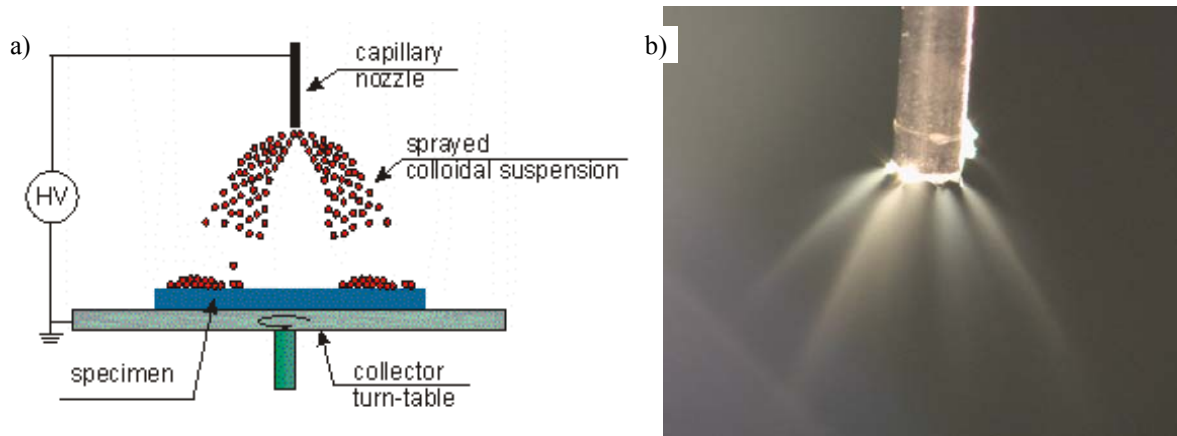


**Fig. 1.** Schematic of thin film deposition by ESD method in multi-jet mode (a), a photography of spray plume in multi-jet mode (b)

After deposition, the specimens with thin film were heat treated at 300°C for 1 h, at 1000 and at 1200°C for 3 h in Nabertherm L3/11 furnace. After thermal treatment the specimens were investigated using SEM microscope EVO-40 (Zeiss) equipped with BRUKER AXS Quantax 200 spectrometer with detector SDD X-flash 5010, 10 mm<sup>2</sup>, 125 eV, operating at 20 kV. Then, half of the specimens underwent thermal tests that comprised of multiple heating and cooling cycles. One thermal cycle comprised of heating to a temperature of 1000°C for 5 h, annealing at this temperature for 4 h, and cooling to a temperature of 100°C within furnace. The thermal test consists of 35 thermal cycles. After 5, 20 and 35 thermal cycles the morphology and elemental composition of the specimens were studied.

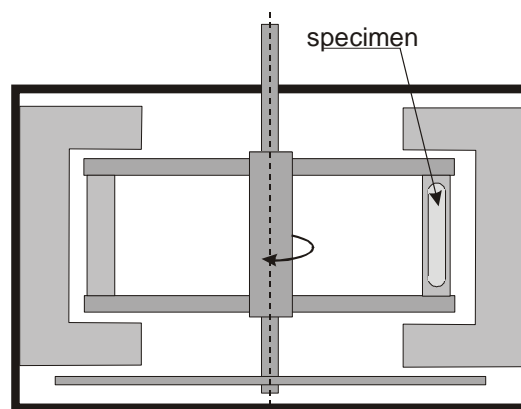


**Fig. 2.** Slurry test rig

The investigation of slurry resistance was performed using slurry erosion test rig shown in Fig. 2 that was built based on the original rig devised by Gandhi and Borse [11]. Slurry tests were carried out with a mean peripheral speed of the rotating sample of  $5 \text{ m s}^{-1}$ . As an erodent was used steel grit of  $530 \mu\text{m}$  diameter and hardness of 51 HRC (458 g per tank - 6 l). As a carrier liquid was used tap water. Because of high aggressiveness of erodent impacts, the initial exposure time was chosen for 30 s, and then the exposure time was extended to 60 s. The total time of slurry test was 300 s. Before the tests and after each exposure, the specimens were washed, dried and weighed using an analytical balance of sensitivity of 0.1 mg.

## RESULTS AND DISCUSSION

The morphologies of deposited thin films after thermal treatment are shown in Fig. 3. In all thin films, an outer layer was porous, built from agglomerates of quasi-globular particles, whose size was depended on the temperature of thermal treatment. In the case of specimen sintered at  $1200^\circ\text{C}$ , their morphology differed from others due to a small residue of agglomerates of the film and formation of big grains underneath.

Investigation of elemental composition (Table 1) showed that temperature of thermal treatment after deposition had an influence on a content of elements in the thin films. The content of aluminum was in the range between 20 and 30% and titanium content was in the range between 7 and 8%. Only in case of a surface of the film sintered at  $1200^\circ\text{C}$  the content of aluminum and titanium was lower. In all specimens were detected substrate elements (iron, chromium and manganese). In the case of the  $\text{Al}_2\text{O}_3 + \text{TiO}_2$  film annealed at  $300^\circ\text{C}$ , the detection of substrate elements was probably connected with low thickness and fluffy structure. Sintering of the coatings caused an increase of substrate elements in the surface layer due to the process of diffusion, especially during sintering at  $1200^\circ\text{C}$ . Thus, visible grains in Fig. 3f were likely the grains of scale that was formed during oxidation of elements of substrate and sintering with the  $\text{Al}_2\text{O}_3 + \text{TiO}_2$  film. Taking into account that  $\text{Al}_2\text{O}_3$ ,  $\text{Cr}_2\text{O}_3$ ,  $\alpha\text{-Fe}_2\text{O}_3$  and  $\text{Ti}_2\text{O}_3$  have the same crystallographic structure of  $\text{D}_{5h}^1$  ( $\text{Al}_2\text{O}_3$ ),  $\text{FeO}$ ,  $\text{MnO}$  and  $\text{TiO}$  have the same structure of  $\text{B1}$  ( $\text{NaCl}$ ), and  $\text{Fe}_3\text{O}_4$  and  $\text{Mn}_3\text{O}_4$  have the same structure of  $\text{Hl}_1$  (spinel), it is likely that during sintering are formed the compounds of three different crystallographic structures: the structure of  $\text{D}_{5h}^1$  ( $\text{Al}_2\text{O}_3$ ) may be formed by oxide of (Al, Cr, Fe or Ti), e.g.  $(\text{Al}_x\text{Cr}_{1-x})_2\text{O}_3$ , the structure of  $\text{B1}$  ( $\text{NaCl}$ ) may be formed by oxide of (Fe, Mn or Ti), e.g.  $\text{Fe}_x\text{Mn}_{1-x}\text{O}$ , the structure of  $\text{Hl}_1$  (spinel) may be formed by oxide of (Fe and Mn), e.g.  $\text{Fe}_x\text{Mn}_{3-x}\text{O}_4$ . Formation of  $(\text{Al}_x\text{Cr}_{1-x})_2\text{O}_3$  can be treated as desirable for heat-resistant coatings, due to its good mechanical properties, high thermal stability and chemical inertness. Oxides, like  $\text{Fe}_x\text{Mn}_{1-x}\text{O}$  or  $\text{Fe}_x\text{Mn}_{3-x}\text{O}_4$  are the products of high temperature oxidation of substrate elements, so their presence is not desired.

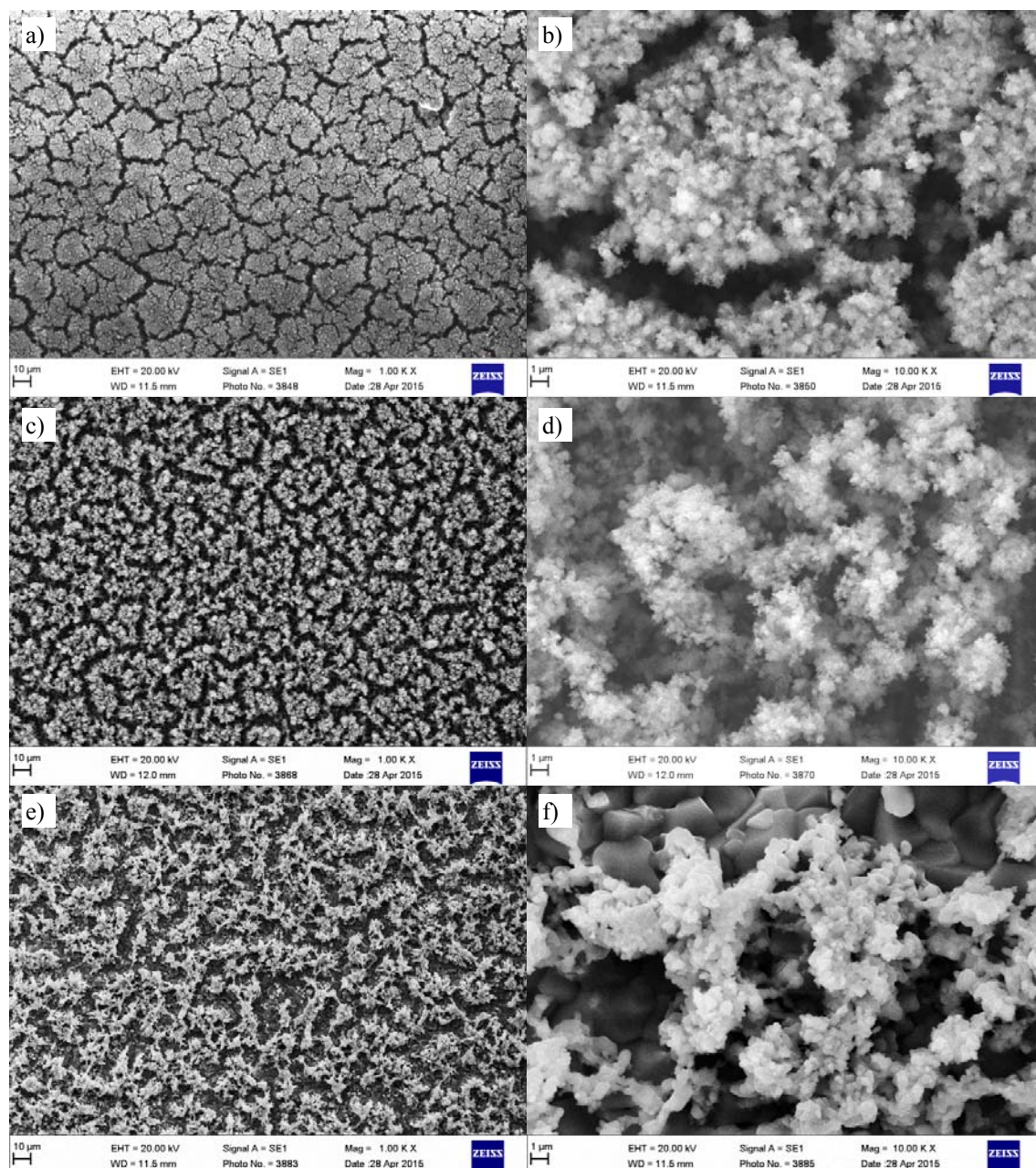


Fig. 3.  $Al_2O_3 + TiO_2$  thin film after thermal treatment at 300°C (a,b), 1000°C (c,d), 1200°C (e,f)

Table 1. Elemental composition of  $Al_2O_3 + TiO_2$  thin film after thermal treatment

|           | T=300°C      |              |            |              |              |            | T=1000°C     |              |            |              |              |            | T=1200°C     |              |            |              |              |            |
|-----------|--------------|--------------|------------|--------------|--------------|------------|--------------|--------------|------------|--------------|--------------|------------|--------------|--------------|------------|--------------|--------------|------------|
|           | surface      |              |            | agglomerate  |              |            | surface      |              |            | agglomerate  |              |            | surface      |              |            | agglomerate  |              |            |
|           | [norm. wt.%] | [norm. at.%] | Error in % | [norm. wt.%] | [norm. at.%] | Error in % | [norm. wt.%] | [norm. at.%] | Error in % | [norm. wt.%] | [norm. at.%] | Error in % | [norm. wt.%] | [norm. at.%] | Error in % | [norm. wt.%] | [norm. at.%] | Error in % |
| Carbon    | 4.39         | 7.62         | 1.00       | 4.07         | 6.96         | 0.95       | 3.20         | 6.32         | 0.76       | 3.49         | 6.15         | 0.86       | 2.37         | 5.33         | 0.65       | 2.75         | 5.13         | 0.76       |
| Oxygen    | 47.64        | 62.37        | 5.81       | 49.02        | 64.04        | 6.03       | 36.27        | 55.16        | 4.33       | 48.01        | 63.50        | 5.78       | 33.70        | 56.89        | 4.38       | 44.81        | 62.82        | 5.79       |
| Aluminium | 28.53        | 22.15        | 1.40       | 27.13        | 21.02        | 1.35       | 24.47        | 22.07        | 1.15       | 27.98        | 21.95        | 1.36       | 11.60        | 11.62        | 0.62       | 23.84        | 19.82        | 1.24       |
| Titanium  | 7.80         | 3.41         | 0.25       | 7.17         | 3.13         | 0.24       | 6.63         | 3.37         | 0.21       | 8.19         | 3.62         | 0.26       | 5.02         | 2.83         | 0.18       | 7.09         | 3.32         | 0.25       |
| Chromium  | 2.83         | 1.14         | 0.11       | 2.49         | 1.00         | 0.11       | 7.22         | 3.38         | 0.22       | 3.36         | 1.37         | 0.13       | 9.94         | 5.17         | 0.32       | 4.58         | 1.98         | 0.17       |
| Manganese | -            | -            | -          | -            | -            | -          | 2.83         | 1.25         | 0.11       | 1.44         | 0.55         | 0.08       | 6.93         | 3.41         | 0.23       | 2.18         | 0.89         | 0.10       |
| Iron      | 8.81         | 3.30         | 0.28       | 10.12        | 3.79         | 0.32       | 19.38        | 8.44         | 0.54       | 7.53         | 2.85         | 0.24       | 30.35        | 14.68        | 0.89       | 14.42        | 5.79         | 0.45       |



**Table 2.** Elemental composition of  $\text{Al}_2\text{O}_3 + \text{TiO}_2$  thin film after thermal cycles

| Temperature      | 300°C    |          |          | 1000°C   |          |          | 1200°C   |          |          |
|------------------|----------|----------|----------|----------|----------|----------|----------|----------|----------|
| Number of cycles | 5        | 20       | 35       | 5        | 20       | 35       | 5        | 20       | 35       |
| Oxygen           | 40.8±5.1 | 41.6±4.7 | 51.0±5.6 | 35.4±4.5 | 38.6±4.6 | 40.4±5.0 | 33.7±4.4 | 32.5±4.2 | 32.2±4.2 |
| Aluminium        | 37.4±1.8 | 29.6±1.4 | 34.1±1.5 | 31.8±1.6 | 35.9±1.7 | 34.6±1.7 | 22.8±1.2 | 17.2±0.9 | 17.3±0.9 |
| Titanium         | 5.6±0.2  | 0.6±0.1  | 8.2±0.3  | 3.7±0.1  | 4.6±0.2  | 5.0±0.2  | 5.2±0.2  | 5.2±0.2  | 3.2±0.1  |
| Chromium         | 2.9±0.1  | 5.7±0.2  | 4.9±0.2  | 6.2±0.2  | 4.8±0.2  | 4.2±0.2  | 4.4±0.2  | 5.6±0.2  | 4.7±0.2  |
| Manganese        | 0.6±0.1  | 1.1±0.1  | 0.4±0.1  | 1.5±0.1  | 1.5±0.1  | 1.3±0.1  | 6.9±0.2  | 17.2±0.5 | 11.7±0.4 |
| Iron             | 9.6±0.3  | 18.3±0.5 | 19.5±0.6 | 18.5±0.6 | 14.6±0.4 | 11.1±0.3 | 24.6±0.7 | 19.8±0.6 | 28.6±0.8 |

Thermal cycles did not cause any crack or any change in the  $\text{Al}_2\text{O}_3 + \text{TiO}_2$  film morphology. EDS investigations showed that thermal cycles had an effect on the change of elemental composition of the films (Table 2). An increase of a content of substrate elements (iron, chromium, manganese) along with an increase of thermal cycles occurred in the case of  $\text{Al}_2\text{O}_3 + \text{TiO}_2$  film annealed at 300°C, probably due to very porous structure, oxidation and diffusion process. In case of the  $\text{Al}_2\text{O}_3 + \text{TiO}_2$  film, sintered at 1000°C the increase of thermal cycles caused a decrease of content of substrate elements. This indicated that the  $\text{Al}_2\text{O}_3 + \text{TiO}_2$  film become more compact nearby the substrate and protected the substrate against oxidation. In case of the  $\text{Al}_2\text{O}_3 + \text{TiO}_2$  film sintered at 1200°C, content of substrate elements after each series of thermal cycles varied significantly. The reason for this might be occurrence of places of film delamination or selective oxidation of an outer layer, or both reasons.

The results of slurry test in the form of slurry erosion curves are shown in Fig. 4. The best resistance against dynamic loading had the  $\text{Al}_2\text{O}_3 + \text{TiO}_2$  film sintered at 1000°C that was not subjected to thermal cycles. Taking into account that  $\text{Al}_2\text{O}_3 \cdot \text{TiO}_2$  is excellent wear and thermal resistant [12,13], good slurry resistance of this film was probably caused by formation of  $\text{Al}_2\text{O}_3 + \text{TiO}_2$  during sintering. Although thermal cycles decreased the slurry erosion resistance of this film, the  $\text{Al}_2\text{O}_3 + \text{TiO}_2$  film sintered at 1000°C and subjected to thermal test had better endurance than the  $\text{Al}_2\text{O}_3 + \text{TiO}_2$  film sintered at 1200°C or annealed at 300°C. The thermal test decreased also slurry endurance of the  $\text{Al}_2\text{O}_3 + \text{TiO}_2$  film sintered at 1200°C. Thermal cycles lowered endurance of the sintered  $\text{Al}_2\text{O}_3 + \text{TiO}_2$  film probably due to decrease of the film adhesion. Taking into account the change of elemental composition of this film, caused by thermal cycles, low endurance of this film against dynamic loading might be caused by weak adhesion of an oxide layer. Only in the case of the  $\text{Al}_2\text{O}_3 + \text{TiO}_2$  film annealed at 300°C thermal cycles increased film endurance. Annealing at 1000°C during each thermal cycle might initiate the sintering process in each cycle.

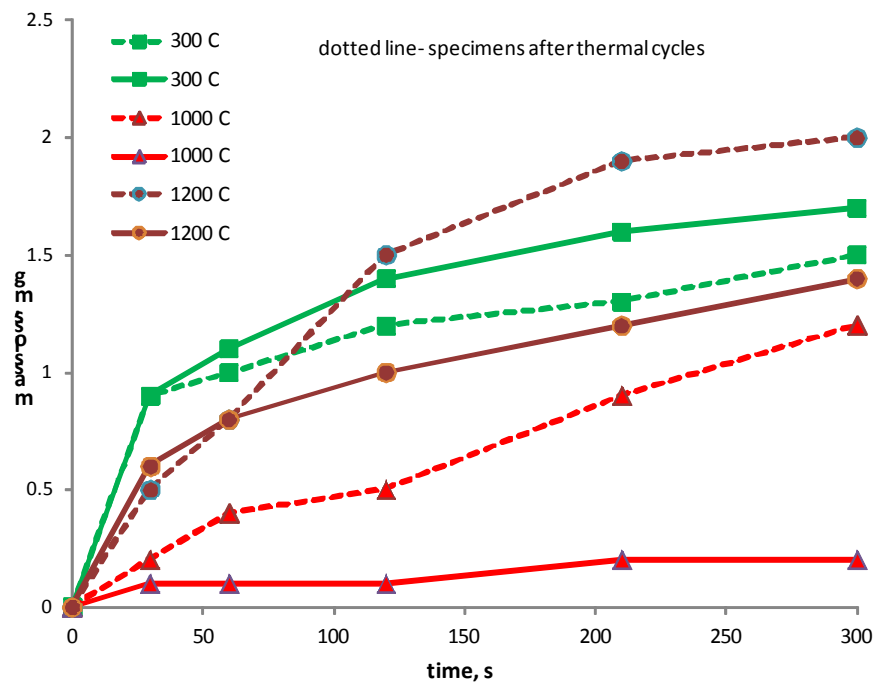
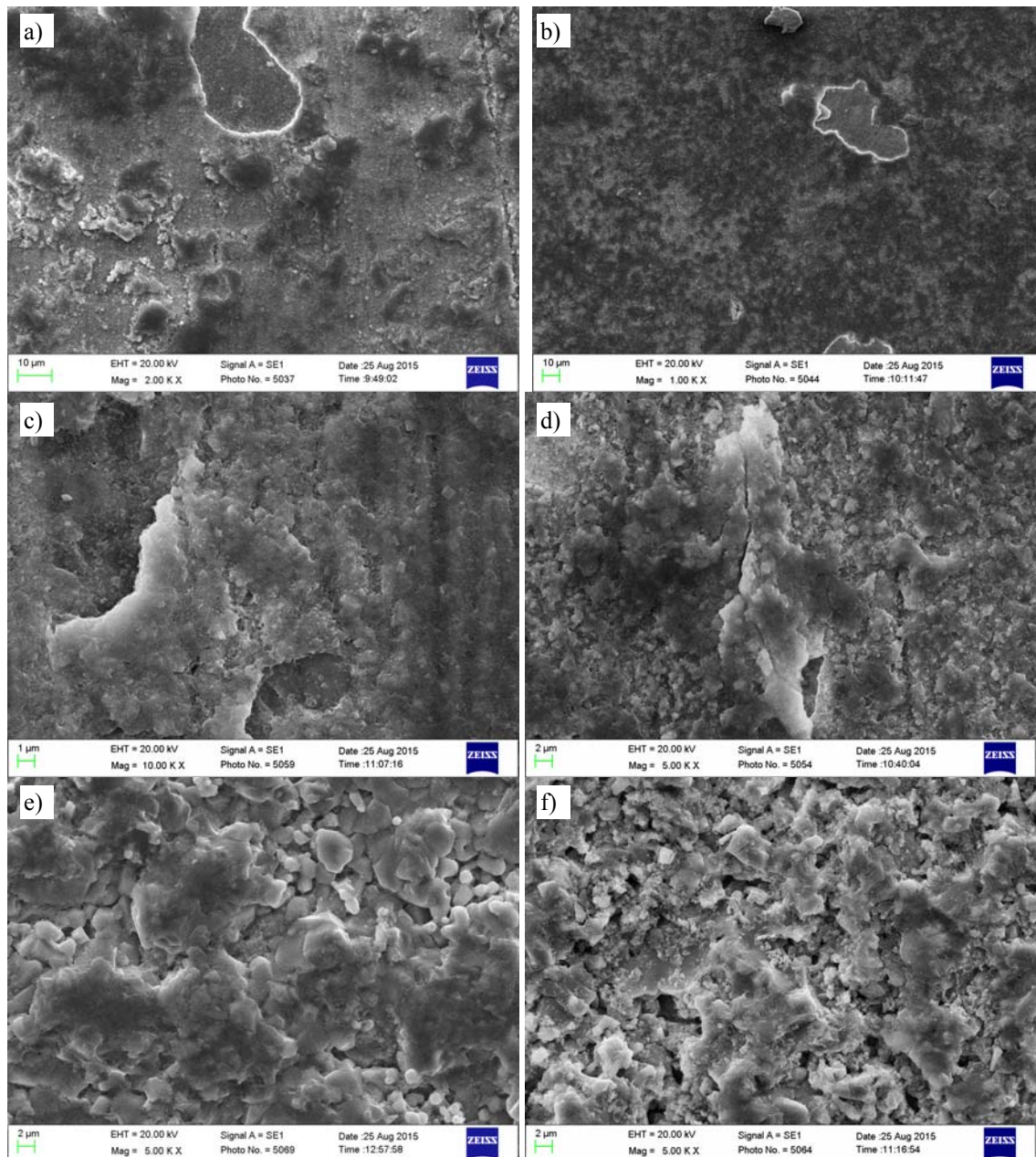


Fig. 4. Slurry erosion curves

Microscopic investigations (Fig. 5) showed that a porous outer layer, visible in Fig. 3, was removed, revealing compact thin film. This indicated that EHDA method allowed deposition of thin film, whose structure changed with the film thickness: close to substrate the film was compact and with an increase of the film thickness the porous layer was formed. The outer layer was porous, built from quasi-globular particles.

The  $Al_2O_3 + TiO_2$  films subjected to impacts of solid particles degraded via development of brittle fracture. However, in the case of  $Al_2O_3 + TiO_2$  film sintered at  $1200^\circ C$ , degradation developed mostly by the brittle fracture of fragments of film with some scale grains lying underneath. Later on, erosion developed by brittle removal of sintered scale grains. Taking into account the slurry curves (Fig. 4) and the morphology of eroded specimen (Fig. 5e), the scale grains, that were weakly adherent to the substrate, decreased the endurance of the film.

Performed investigations indicated that thermal cycles decreased the film endurance due to delamination of coatings. In Figs 5 b and d are shown the places of film delamination. Brittle thin film that is not supported by substrate cannot withstand impact and easily fractures at little impact energy. The brittle crack growth needs even less energy. Thus, with an increase of the area of delamination of the film, increased the rate of degradation. In case of the  $Al_2O_3 + TiO_2$  film sintered at  $1200^\circ C$ , high erosion rate was likely caused by increasing scale lying underneath the film that had little dynamic endurance. Thus, deposition of the  $Al_2O_3 + TiO_2$  film did not protect the substrate against oxidation at  $1200^\circ C$ .



**Fig. 5.** The  $\text{Al}_2\text{O}_3 + \text{TiO}_2$  thin film after slurry tests, (a,b) annealed at  $300^\circ\text{C}$ , (c,d) sintered at  $1000^\circ\text{C}$ , (e,f) sintered at  $1200^\circ\text{C}$ : (b,d,f) thin films subjected to thermal cycles

## CONCLUSIONS

Performed investigations showed that:

- The structure of the  $\text{Al}_2\text{O}_3 + \text{TiO}_2$  film made from of colloidal suspension of  $\text{TiO}_2$  nanoparticles in 3% solution of  $\text{Al}(\text{NO}_3)_3 \cdot 9\text{H}_2\text{O}$  in ethanol ( $\text{C}_2\text{H}_5\text{OH}$ , 99.9%) deposited by EHDA method onto ferritic X10CrAlSi18 steel changed with the film thickness.
- Thermal treatment after film deposition had influence on film resistance against oxidation during thermal cycles and slurry erosion.



- The best protective properties had the  $Al_2O_3 + TiO_2$  film sintered at 1000°C. This coating protected the substrate against oxidation during thermal cycles and had the best resistance against slurry erosion.
- Sintering the  $Al_2O_3 + TiO_2$  film at 1200°C caused formation of scale underneath the film that increased the film-substrate system degradation.

### ACKNOWLEDGEMENTS

The paper is supported by the Project No. 2011/03/B/ST8/05643 "The elaboration of coatings of heat resistant properties deposited by means of electrohydrodynamic method" financed by Polish National Science Centre.

### REFERENCES

1. Neagu R., Perednis D., Princiville A., Djurado E.; Zirconia coatings deposited by electrostatic spray deposition. Influence of the process parameters. *Surface and Coatings Technology* 200 (2006), 6815-6820.
2. da Conceição L., Dessemond L., Djurado E., Muccillo E.N.S.;  $La_{0.7}Sr_{0.3}MnO_3 - \delta$  barrier for  $Cr_2O_3$ -forming SOFC interconnect alloy coated by electrostatic spray deposition. *Surface and Coatings Technology* 254 (2014), 157-166.
3. Bagley R. D., Cutler I.B., Johnson D. L., Effect of  $TiO_2$  on initial sintering of  $Al_2O_3$ , *Journal of the American Ceramic Society* 53 (1970), 136–141.
4. Bose K., Wood R.J.K., Wheeler D.W.: High energy solid particle erosion mechanisms of superhard CVD coatings. *Wear* 259 (2005), 135–144.
5. Tabakoff W.: Erosion resistance of superalloys and different coatings exposed to particulate flows at high temperature. *Surface and Coatings Technology* 120–121 (1999), 542–547.
6. Knuuttila J., Ahmaniemi S., Mantyla T.: Wet abrasion and slurry erosion resistance of thermally sprayed oxide coatings. *Wear* 232 (1999), 207–212.
7. Grewal H. S., Agrawal A., Singh H., Shollock B. A.: Slurry Erosion Performance of Ni- $Al_2O_3$  Based Thermal-Sprayed Coatings: Effect, of Angle of Impingement. *Journal of Thermal Spray Technology* 23(3) (2014), 389 – 401.
8. Tu J.P., Zhu L.P., Zhao H.X.: Slurry erosion characteristic of TiN coatings on alfa-Ti and plasma nitrided Ti alloy substrates. *Surface and Coatings Technology* 122 (1999), 176-182
9. Al-Bukhaiti M.A., Ahmed S.M., Badran F.M.F., Emara K.M.: Effect of impingement angle on slurry erosion behaviour and mechanisms of 1017 steel and high-chromium white cast iron. *Wear* 262 (2007), 1187-1198.
10. Lathabai S., Pender D.C.: Microstructural influence in slurry erosion of ceramics. *Wear* 189 (1995), 122-135.
11. Gandhi B. K., Borse S. V.: Nominal particle size of multi-sized particulate slurries for evaluation of erosion wear and effect of fine particles. *Wear* 257 (2004), 73–79.
12. Bian H., Yang Y., Wang Y., Tian W.: Preparation of nanostructured alumina–titania composite powders by spray drying, heat treatment and plasma treatment, *Powder Technology* 219 (2012), 257–263.
13. Wang Y., Jiang S., Wang M., Wang S., Xiao T.D., Strutt P.R.: Abrasive wear characteristics of plasma sprayed nanostructured alumina/titania coatings, *Wear* 237 (2000), 176-185.